Journal of Marine Research, 58, 957–982, 2000

Buoyancy-forced circulations around islands and ridges

by Michael A. Spall[1]

ABSTRACT

Observations, theory, and modeling studies indicate that dominant components of both the upwelling and downwelling limbs of the thermohaline circulation take place near boundaries and in regions of steep and/or rough topography. Analytic and numerical results are used here to show that the interaction of upwelling regions with lateral boundaries fundamentally alters the resulting large-scale circulation compared to cases of open ocean upwelling. For narrow upwelling regions, viscous fluxes emerge as a leading term in the potential vorticity budget. The strong horizontal recirculation gyres that are found for sub-basin-scale open ocean upwelling (β-plumes) are replaced by weak, unidirectional flow into or out of the region of vertical motion. If the upwelling is located near an island or mid-ocean ridge, potential vorticity budgets require that a strong, large-scale recirculation develop around the topography, sometimes far from the region of mixing. The resulting boundary layers provide an important dynamic link between the large-scale horizontal components of the thermohaline circulation and the small-scale regions of strong vertical motions.

1. Introduction

Diapycnal mixing in the ocean abyss is a central component of the meridional overturning circulation and the global budgets of energy, heat, fresh water, and tracers. While recent tracer and microstructure measurements suggest that diapycnal mixing is small in the stratified ocean interior (Ledwell *et al.,* 1993; Polzin *et al.,* 1997), evidence suggests that strong turbulent mixing is concentrated near boundaries and in regions of steep or rough topography. The importance of mixing near boundaries was suggested by the early works of Munk (1966) and Armi (1978). Recent observational studies have pointed to a number of specific regions where boundary mixing is dominant, including turbulent entrainment into descending dense water overflows (Price and Baringer, 1994); mixing near mid-ocean ridges (Polzin *et al.,* 1997); mixing near seamounts (Toole *et al.,* 1997); mixing near boundaries (Ledwell and Hickey, 1995); and mixing in narrow channels connecting adjacent abyssal basins (Ferron *et al.,* 1998). These previous observational studies have concentrated on estimating the magnitude of the mixing and describing its effects on the properties of the water masses involved.

Strong diapycnal mixing also takes place in the upper limb of the meridional overturning circulation where warm waters are cooled through heat loss to the atmosphere. Descriptive

1. Woods Hole Oceanographic Institution, Department of Physical Oceanography, Woods Hole, Massachusetts, 02543, U.S.A. ***email: mspall@whoi.edu***

studies of the large-scale circulation have often assumed that such sites of deep convective mixing in the basin interior are coincident with the downwelling limb of the thermohaline circulation (e.g., Schmitz and McCartney, 1993). However, Spall and Pickart (2000) use both theory and numerical models to show that the buoyancy-forced downwelling in the surface mixed layer is concentrated near lateral boundaries and that flows in the basin interior that are subject to cooling remain nearly horizontal.

Given the growing body of evidence that buoyancy-forced upwelling and downwelling are concentrated near lateral boundaries, it is of interest to understand the consequences of vertical motions near lateral boundaries on the large-scale circulation. Stommel (1982) and Joyce and Speer (1987) recognized that a local region of vertical motion in a basin interior would result in a strong, large-scale circulation through the influence of the meridional gradient of planetary vorticity. As will be discussed further in this paper, in the absence of viscous effects, the variation in the Coriolis parameter with latitude requires strong horizontal recirculations, often called β-plumes, to balance weak vertical motions. The strength of the recirculation compared to the strength of the upwelling scales as the ratio of the meridional scale of the upwelling region to either the radius of the earth (spherical coordinates, Pedlosky, 1996) or the distance from the equator (beta-plane, Spall, 1999). In each of these studies, the dynamics are planetary geostrophic, meridional gradients of the planetary vorticity are crucial, and topographic and boundary effects are neglected.

Recent results from basin-scale primitive equation (Jia, 2000) and quasi-geostrophic (Ozgokmen *et al.,* 2000) general circulation models suggest that entrainment into the descending dense water overflow through the Strait of Gibraltar may be responsible for the eastward-flowing Azores Current and westward-flowing Azores Counter Current. This is an example of a case where local diapycnal mixing can generate basin-scale circulations in the upper ocean. Although this flow structure is qualitatively similar to what one would expect from the simple open ocean mixing β-plume model, the strength of the horizontal circulations found in these general circulation models, and of the Azores Current, is much less than one would expect from the simple inviscid theory. The proximity of steep topography to the turbulent entrainment into this, and other, overflows suggests that boundary effects are likely to be important.

These previous theoretical, observational, and modeling studies indicate that understanding the dynamical constraints that arise when turbulent diapycnal mixing and/or vertical motions are concentrated near lateral boundaries is important to understanding how both the downwelling and upwelling limbs of the thermohaline circulation are maintained. The present study extends these previous open ocean theories by considering the influences of lateral boundaries and multiply connected domains on the large-scale circulation resulting from regions of localized upwelling or downwelling. It is shown that, as the mixing is confined to regions close to a boundary, lateral viscosity becomes important to leading order in the potential vorticity budget. This has important consequences for the circulation both near and far from the mixing region. In the case of multiply connected domains (intended here to represent islands or abyssal ridge systems), isolated mixing near

topography can force a strong, large-scale exchange between adjacent basins, far from the mixing regions, even when the gaps connecting the basins are narrow.

2. Dynamical framework and boundary effects

It is useful to begin the discussion with a review of the basic circulation that results from a region of localized upwelling in a two-layer, flat bottom, inviscid ocean subject to planetary geostrophic dynamics on a β-plane. While the general conclusions are similar to those of Stommel (1982) and Pedlosky (1996), this foundation provides a familiar starting point from which to introduce the major new elements of this study: lateral boundaries and multiply connected domains. The intent here is to provide estimates of the large-scale circulation structure and strength and a physical interpretation of the basic mechanisms at work.

Consider a rectangular region of zonal extent L and meridional extent L_y with uniform upwelling[2] from below of strength w (Fig 1). For a fluid that satisfies the planetary geostrophic momentum balance on a β-plane, the linear vorticity balance for the upper layer requires a southward flow within the region of upwelling,

$$v = -\frac{fw}{\beta H}, \tag{1}$$

where the Coriolis parameter $f = f_0 + \beta y$, β is the meridional gradient of f, and H is the thickness of the fluid layer. The meridional flow just to the north of the upwelling region must be zero so that all of the southward flow at the northern limit of upwelling is provided by a zonal jet extending from the west (assuming no flow through the eastern boundary and that eastern boundary layers are unimportant). The transport carried in this eastward flowing jet is readily calculated to be

$$M_n = H \int_{x_e}^{x_w} v\, dx = \frac{f_n W}{\beta L_y}, \qquad W = wLL_y \tag{2}$$

where W is the total amount of upwelled water and f_n is the Coriolis parameter at the northern limit of upwelling. Similar considerations at the southern limit of the upwelling region produce a weaker westward flowing jet of strength $M_s = f_s W/\beta L_y$.

The mass balance is closed by a weak westward flow between y_s and y_n. The dynamic pressure at the western edge of the upwelling region may be calculated, making use of (1), geostrophy, and the boundary condition $P = 0$ at $x = x_e$, as

$$P = \int_{x_e}^{x_w} fv\, dx = \frac{f^2 wL}{\beta H}. \tag{3}$$

2. The large-scale dynamical influences of diapycnal mixing are represented here by imposing a vertical mass flux w. The implicit assumption in this traditional approach is that a one-dimensional heat balance exists such that the vertical advection is balanced by a vertical diffusion in the density equation. The advantage of this approach is that the details of the turbulent mixing process need not be explicitly resolved.

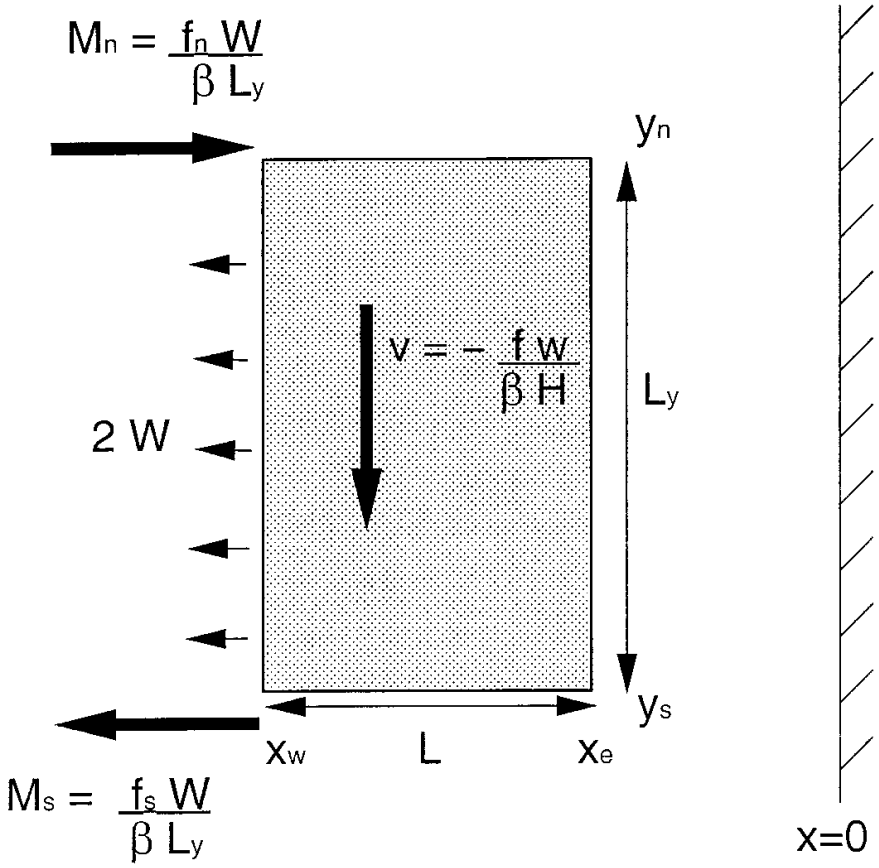

Figure 1. Schematic of the upper ocean flow pattern forced by upwelling from below in the open ocean. The region of upwelling strength w measures L by L_y. The upwelling forces zonal jets of strength $M_n = f_n W/\beta L_y$ and $M_s = f_s W/\beta L_y$ where $W = wLL_y$ is the total amount of upwelled water. Meridional variations in pressure along the western edge of the upwelling region drive a weak uniform westward flow with transport $2W$.

Because the Coriolis parameter is a function of y, the dynamic pressure is also a function of y. This pressure gradient on a beta-plane results in a uniform zonal flow to the west, as indicated in Figure 1. The total transport carried in this westward flow, with $f = f_0 + \beta y$, is

$$U = -H \int_{y_s}^{y_n} u \, dy = -H \int_{y_s}^{y_n} \frac{1}{f} \frac{\partial P}{\partial y} \, dy = -2W. \tag{4}$$

If the strength of the horizontal recirculation gyre M is taken as the average of the northern and southern jets, the ratio of the horizontal gyre to the upwelling strength is

$$\frac{M}{W} = \frac{f_n + f_s}{2\beta L_y}. \tag{5}$$

Weak upwelling events can force strong horizontal recirculation gyres if the meridional scale of the upwelling is small. It is anticipated that additional processes, such as nonlinearities, instabilities, or dissipation, may become important as the meridional scale of the upwelling region becomes very small.

It is also instructive to consider the same circulation in terms of conservation of vorticity and conservation of mass. If one integrates the momentum equation tangential to a contour encircling the upwelling region, assuming a linear, steady solution, it is required that the net flux of planetary vorticity into the upwelling region be zero.

$$\int_C f\,\mathbf{v}\cdot\mathbf{n}\,ds = 0. \tag{6}$$

The unit normal vector is denoted by $\mathbf{n}$ and s is the distance along the contour. For mid-latitude regimes, f is always of the same sign so that in order for the integral to be satisfied $\mathbf{v}\cdot\mathbf{n}$ must change sign. This means that the flow cannot be uniformly out of the upwelling region. If it is assumed that there is no flow through the eastern boundary, then the vorticity budget requires a horizontal recirculation. This is the essential mechanism of the beta-plume discussed by Stommel (1982), Joyce and Speer (1987), and Pedlosky (1996).

This integral may be written in terms of the above transports as

$$M_n f_n = M_s f_s + W(f_n + f_s). \tag{7}$$

Conservation of mass requires that

$$\int_C \mathbf{v}\cdot\mathbf{n}\,ds = 0. \tag{8}$$

This may be written for the uniform upwelling case as

$$M_s + 2W = M_n + W. \tag{9}$$

Combining (7) and (9) gives an estimate of the northern jet strength M_n, nondimensionalized by W, as

$$\frac{M_n}{W} = \frac{f_n}{\beta L_y} = \frac{f_s}{\beta L_y} + 1, \tag{10}$$

which is equivalent to the result derived using a local linear vorticity balance. As the meridional scale of upwelling becomes small, the strength of the recirculation gyre increases. The flux of planetary vorticity carried by the net mass flux into the upwelling region, fW, is balanced by the meridional flux divergence arising from the small variation in f with latitude.

The utility of the potential vorticity budget becomes clear when the influences of lateral boundaries are included. Consider the case where uniform upwelling is confined to a region of width L adjacent to an eastern boundary ($x_e = 0$ in Fig. 1). A potential vorticity budget around a contour that encloses the upwelling region will now include a contribution from the viscous eastern boundary layer. In order to calculate the potential vorticity flux into the eastern boundary, the structure of the meridional velocity within the viscous boundary layer in the vicinity of the upwelling region must first be determined.

It is useful to consider the case of a steady, linear, homogeneous, quasi-geostrophic fluid subject to an imposed vertical velocity at the surface (representing the diapycnal mass flux). It is assumed that the meridional extent of the upwelling region is large compared to the zonal extent, so that meridional derivatives of all variables are negligible. Two forms of dissipation are considered here, lateral diffusion and a linear bottom drag. The nondimensional potential vorticity equation may be written in terms of the transport streamfunction as

$$\psi_x - w_z = (\delta/L)^3\psi_{xxxx} + (\delta_s/L)\psi_{xx} \tag{11}$$

where $\delta = (A_h/\beta)^{1/3}$ is the Munk layer thickness, $\delta_s = C_D/\beta$ is the Stommel layer thickness, A_h is a lateral viscosity coefficient, and C_D is a linear bottom drag coefficient. The streamfunction has been nondimensionalized by $f_0W/\beta L_y$, the transport forced by uniform upwelling of strength w, and x has been nondimensionalized by the upwelling width L. The upwelling strength $w = 1$ is uniform within $-1 < x < 0$ and zero for $x < -1$.

a. Munk layer

The solution to (11) is obtained by representing the streamfunction as the sum of the inviscid solution and boundary layers that are required to satisfy boundary conditions at the eastern wall and at the western edge of the upwelling region. The case where lateral friction dominates over bottom drag, $\delta \gg \delta_s$, is considered first. It is useful to define the total streamfunction ψ as the sum of a forced, inviscid solution Ψ and an unforced, viscous solution ϕ,

$$\psi = \Psi + \phi, \tag{12}$$

where Ψ satisfies

$$\Psi_x - w_z = 0. \tag{13}$$

Substitution of (12) into (11), and making use of (13) results in the unforced, viscous equation that must be satisfied by each of the boundary layers in the problem. No assumption has been made about the size of δ/L.

$$\phi_x = (\delta/L)^3\phi_{xxxx}. \tag{14}$$

In the directly forced region, three boundary layers need to be considered, one that decays exponentially toward the west from the eastern boundary, and two that decay exponentially toward the east from $x = -1$. In the unforced region, there is one solution that decays westward from $x = -1$. However, since the upwelling region may be narrower than the Munk layer, the westward decaying boundary layer originating at the eastern boundary may also extend well into the unforced region.

The solution requires that the total streamfunction ψ and its first three derivatives match at $x = -1$. A final boundary condition applies on the eastern wall, where either free-slip or

no-slip conditions may be imposed. The solution procedure is similar to the standard approach for eastern and western boundary layers adjacent to solid boundaries as found, for example, in Pedlosky (1987, pages 253–269) and is not reproduced in detail here.

The solution for the transport streamfunction with no-slip boundary conditions imposed on the eastern wall is broken up into two parts: one for the region where $w \neq 0$ and one for the area to the west of the upwelling region. The streamfunction to the west of the upwelling region ($x < -1$) is given by

$$\psi = C_0 - 1 + \frac{1}{3}\frac{\delta}{L}[e^{[(x+1)L]/\delta} + (2\cos\alpha e^{-(L/2\delta)} - 3)\, e^{(xL/\delta)}], \tag{15}$$

where the constant $\alpha = \sqrt{3}L/2\delta$.

In the directly forced region ($-1 < x < 0$), the streamfunction is

$$\psi = C_0 + x + \frac{1}{3}\frac{\delta}{L} \times [\cos\alpha(x+1) - \sqrt{3}\sin\alpha(x+1))e^{-[(x+1)L]/2\delta} + (2\cos\alpha e^{-(L/2\delta)} - 3)\, e^{(xL/\delta)}]. \tag{16}$$

The constant of integration C_0 is chosen to set the streamfunction to zero on the eastern boundary,

$$C_0 = -\frac{\delta}{L}\left[\left(\cos\alpha - \frac{\sqrt{3}}{3}\sin\alpha\right) e^{-(L/2\delta)} - 1\right]. \tag{17}$$

A similar approach may be used to solve for the streamfunction for free-slip boundary conditions on the eastern wall:

$$\psi = C_1 - 1 + \frac{1}{3}\frac{\delta}{L}\left[e^{[(x+1)L]/\delta} - e^{-(L/2\delta)}\left(\cos\alpha + \frac{3\sqrt{3}}{2}\sin\alpha\right) e^{(xL)/\delta}\right], \qquad x < -1. \tag{18}$$

and

$$\psi = C_1 + x + \frac{1}{3}\frac{\delta}{L}[\cos\alpha(x+1) - \sqrt{3}\sin\alpha(x+1))\, e^{[-(x+1)L]/2\delta} - e^{-(L/2\delta)}\left(\cos\alpha + \frac{3\sqrt{3}}{2}\sin\alpha\right) e^{(xL/\delta)}, \qquad -1 < x < 0. \tag{19}$$

The constant of integration required to set the streamfunction to zero on the eastern boundary is

$$C_1 = \frac{5\sqrt{3}}{6}\sin\alpha\, e^{-L/2\delta}. \tag{20}$$

For wide mixing regions ($L/\delta \gg 1$) the standard eastern boundary layer solution is recovered near the eastern boundary. For narrow upwelling regions, where $L/\delta = O(1)$, the boundary layers decaying eastward from the western limit of upwelling (terms proportional to $e^{-(x+1)L/2\delta}$) interact with the eastern boundary. Meridional motion to the west of the upwelling region is forced by lateral diffusion of relative vorticity generated within the upwelling region. The relative vorticity arises both as a result of the eastern boundary condition and directly from the step function in forcing at $x = -1$.

b. Stommel layer

For the case where bottom drag dominates over lateral friction, $\delta_s \gg \delta$, there is only one boundary layer and it decays eastward away from the western limit of upwelling. To the west of the upwelling region ψ is constant, and ψ is also constant along the eastern boundary. The matching condition at $x = -1$ is that $\psi_x = 0$.

Once again, the solution is presented in two parts.

$$\psi = 1 - \frac{\delta_s}{L}(1 - e^{-L/\delta_s}), \qquad x < -1 \tag{21}$$

$$\psi = -x - \frac{\delta_s}{L}(e^{-(x+1)L/\delta_s} - e^{-L/\delta_s}), \qquad -1 < x < 0. \tag{22}$$

c. Potential vorticity budget near the boundary

An example of the meridional motion induced by a narrow upwelling region of width $L/\delta = 2$ is shown in Figure 2a for both no-slip and free-slip Munk layer solutions as well as for the Stommel layer. The inviscid solution is also given for reference. With no-slip on the eastern boundary, the meridional velocity is maximum within the upwelling region and decays to zero at both the eastern boundary and westward into the unforced region. The free-slip meridional velocity is approximately twice as large in the upwelling region but decays to zero toward the west with the same zonal scale. The meridional motion is confined to the upwelling region for linear bottom drag. The streamfunction is shown in Figure 2b. The meridional transport for the case with free-slip boundary conditions is approximately twice that with no-slip boundary conditions and 75% of the frictionless transport. The transport with bottom drag is intermediate to that with free-slip and no-slip. In the absence of lateral viscosity (the standard open ocean β-plume case discussed earlier) the streamfunction increases uniformly from 0 to 1 over the width of the upwelling region and remains constant to the west of the upwelling region.

The maximum meridional velocity as a function of the upwelling width L/δ is shown in Figure 2c. For wide upwelling regions with lateral viscosity, the maximum meridional velocity is slightly greater than 1. This is analogous to the enhanced meridional transport in a western boundary layer with lateral viscosity that arises from the eastward decaying trigonometric boundary layers. As the upwelling width narrows below approximately 5δ

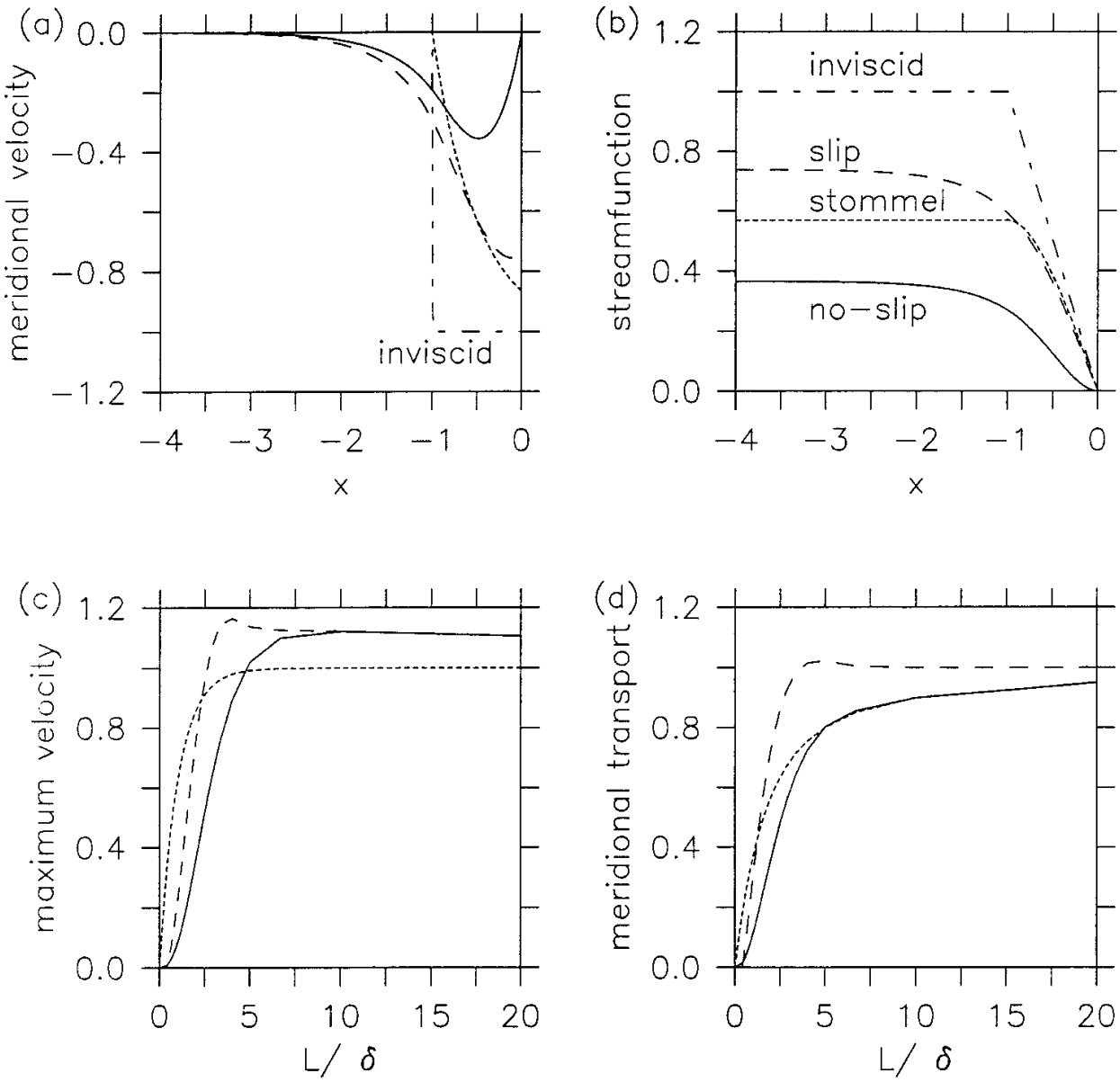

Figure 2. Meridional flow structure forced by upwelling of width 2δ adjacent to an eastern boundary. The boundary is located at $x = 0$, the upwelling is confined to $-1 < x < 0$, where x is nondimensionalized by L. (a) Meridional velocity; (b) meridional transport; maximum meridional velocity (c) and total meridional transport (d) as a function of upwelling width L/δ. Solid line: no-slip; long dashed line: free-slip; short dashed line: Stommel layer; dot-dashed line: inviscid.

the maximum meridional velocity decays rapidly to zero for all frictional parameterizations. The total meridional transport forced by the upwelling is shown in Figure 2d. As expected, the transport approaches 1 for wide upwelling regions. Substantial decreases in meridional transport are found when the zonal scale of the upwelling decreases below 5δ. In the free-slip and no-slip cases, as well as with linear bottom drag, the total meridional transport, and hence the strength of the horizontal recirculation gyre required in the absence of viscosity, decreases to zero as $L/\delta \to 0$.

The question naturally arises as to what balances the flux of planetary vorticity out of the upwelling region when the horizontal recirculation gyre is suppressed by viscosity.

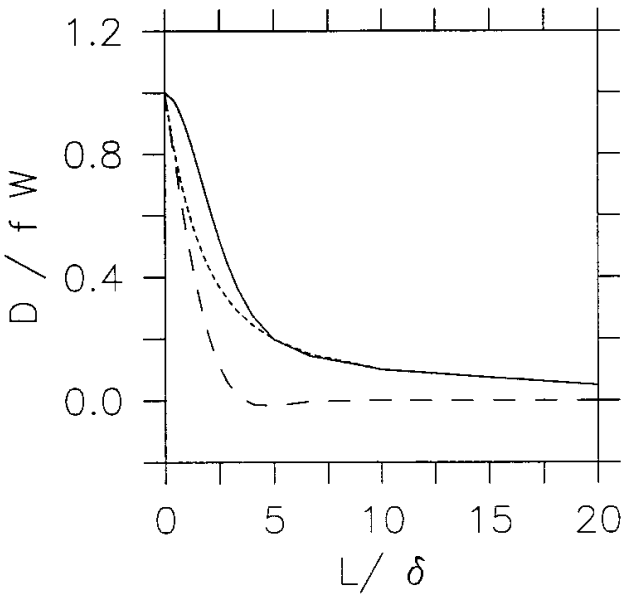

Figure 3. Nondimensional strength of the dissipation D along the eastern boundary as a function of upwelling width for no-slip (solid line), free-slip (long dashed line), and linear bottom drag (short dashed line) dissipation, from Eqs. (23), (24) and (25).

Integration of the momentum equation around the upwelling region gives rise to a viscous term from the interaction of the meridional flow with the eastern boundary. Although the meridional transport goes to zero as $L \to 0$, the viscous terms $A_h v_{xx}$ and $C_D v$ do not go to zero. For the case of no-slip eastern boundary conditions, the viscous term D is

$$D = H \int_{y_s}^{y_n} A_h v_{xx}\, dy = fW \frac{\delta}{L} \left[\left(\cos\alpha - \frac{\sqrt{3}}{3} \sin\alpha \right) e^{-(L/2\delta)} - 1 \right], \tag{23}$$

where H is the thickness of the isopycnal layer. The integral from y_s to y_n is taken at $x = 0$ on the eastern boundary.

The strength of D (nondimensionalized by fW) as a function of the upwelling width is shown in Figure 3. As the upwelling region becomes very narrow ($L/\delta \to 0$), the contribution of the viscous term approaches fW. Recall that this is the net potential vorticity flux balanced by the recirculation gyre in the absence of friction. The contribution to the potential vorticity budget previously supplied by meridional flux divergence of planetary vorticity through a strong horizontal recirculation gyre is now supplied by a viscous flux into the eastern boundary. The mass flux is purely zonal toward the west out of the upwelling region ($v \to 0$, Fig. 2). As the upwelling region becomes wide, the boundary layers that decay eastward from the western limit of upwelling no longer reach the eastern boundary (terms proportional to $e^{-(L/2\delta)}$). In that limit, the contribution due to frictional fluxes into the eastern boundary is the same as for the traditional eastern boundary layer in a large-scale wind driven gyre and decreases as δ/L.

For the case of free-slip on the eastern boundary, the viscous term is

$$D = H \int_{y_s}^{y_n} A_h v_{xx}\, dy = fW \frac{\delta}{L} \frac{2\sqrt{3}}{3} e^{-(L/2\delta)} \sin \alpha. \tag{24}$$

The strength of the free-slip viscous term as a function of the upwelling width is also shown in Figure 3. It is important to remember that the free-slip boundary condition does not imply no vorticity flux into the eastern boundary. For moderate upwelling widths, free-slip has a smaller viscous stress than does no-slip. However, in the limit of very narrow upwelling, the free-slip condition results in exactly the same contribution to the vorticity budget as no-slip and is able to balance the lateral (zonal) flux of planetary vorticity out of the region without the need to develop a strong horizontal recirculation gyre.

The dissipation induced by linear bottom drag is

$$D = H \int_{y_s}^{y_n} C_D v\, dy = fW \frac{\delta_s}{L} (e^{-(L/\delta_s)} - 1). \tag{25}$$

The strength of the bottom drag viscous term as a function of the upwelling width is also shown in Figure 3. For very narrow upwelling widths, the bottom drag case behaves much like the free-slip case, while for wide upwelling regions the bottom drag decays as δ_s/L, as does the no-slip Munk solution.

The zonal mass flux out of narrow upwelling regions provides a clear connection to mass flux into a basin through lateral advection considered by Yang and Price (2000). In the limit of narrow upwelling, the forcing by vertical motions is indistinguishable from the forcing by lateral advection through the boundary. Furthermore, this balance helps to understand the vorticity balance in the downwelling limb of the thermohaline circulation in general circulation models, which is generally concentrated near the lateral boundaries (see Marotzke, 1997; Spall and Pickart, 2000).

d. Examples in a simple numerical model

The basic circulations implied by the above budget considerations are now demonstrated using a 2-layer primitive equation isopycnal model (MICOM). The version used here is a much simplified version of the full model described by Bleck *et al.* (1992). Temperature and salinity are constant within each isopycnal layer and there is no wind-stress or surface buoyancy flux so that there is no active mixed layer. Subgridscale mixing is limited to along-isopycnal Laplacian viscosity. The model is forced by an imposed diapycnal mass flux from layer 2 into layer 1 of uniform strength over a specified region of dimension L by L_y. Mass is balanced by an equal amplitude downwelling imposed near the western boundary. (The essential characteristics of the solution are not sensitive to where this downwelling is located.)

The model domain is 2000 km by 2000 km with uniform grid spacing of 20 km. The layers are each 1000 m thick, giving a total ocean depth of 2000 m. The reduced gravity between the layers is 0.03 m s^{-2} (the general circulation characteristics are not sensitive to this choice). The Coriolis parameter at the mid-latitude of the basin is $f = 10^{-4}$ s^{-1} and $\beta = 2 \times 10^{-13}$ cm^{-1} s^{-1}. The upwelling strength is 10^{12} cm^3 s^{-1} = 1 Sv and the Munk layer thickness is either 20 km or 50 km. The model is initialized at rest and integrated for a period of 10 years, at which point the fields have arrived at a steady state. For all calculations considered here, the nonlinear terms, although included in the calculations, are negligible.

The basic β-plume circulation is demonstrated in Figure 4a for a case with uniform upwelling distributed over a meridional extent of 1540 km and zonal extent of 20 km located at longitude 1500 km. The Munk layer thickness $\delta = 20$ km. The circulation in the upper layer is shown, the deep circulation is of the same strength with opposite sign (linear regime, flat bottom). The flow is dominated by a large-scale recirculation gyre extending westward from the northern and southern limits of the upwelling region. The normalized strength of the recirculation is $M_n/W = 3.82$, in close agreement with the theoretical estimate of $M_n/W = f_n/\beta L_y = 3.75$. The presence of viscosity in the open ocean alters the width of the recirculating jets, but not the total transport. The meridional length scale of the westward jets grows slightly toward the west, in general agreement with the expected $\delta^{3/4}x^{1/4}$ structure. The westward transport in the southern jet is 1 Sv smaller than the eastward transport in the northern jet, as expected based on the linear vorticity balance at the limits of the upwelling region (Eq. (9)). The difference between these jet transports, plus the amount of upwelled water, is 2 Sv and accounted for in the weak westward flow between the zonal jets, consistent with the theory.

The influences of interaction with the eastern boundary are indicated by a case where the upwelling is confined to a 20 km band adjacent to the eastern boundary with no-slip conditions and $\delta = 50$ km (Fig. 4b). The recirculation is essentially eliminated and the flow is now nearly uniform toward the west out of the upwelling region. This is as expected based on (23) for $L/\delta = 0.4$. Frictional effects convert the vertical motion near the boundary into nearly zonal flow without the need to advect parcels across the planetary vorticity gradient. A zonal flow out of the mixing region is found even for upwelling confined to a point source on the eastern boundary. As implied by (23), the strong horizontal recirculation gradually re-emerges as the width of the mixing region is increased (a quantitative comparison between the model and the theory for these intermediate mixing scales is given in the next section).

3. Multiply connected domains: Mixing near islands and ridges

Topographic features such as planetary scale islands, island chains, and abyssal ridge systems act as boundaries between adjacent ocean basins. Understanding what drives the transport between ocean basins is a fundamental quest of large-scale physical oceanogra-

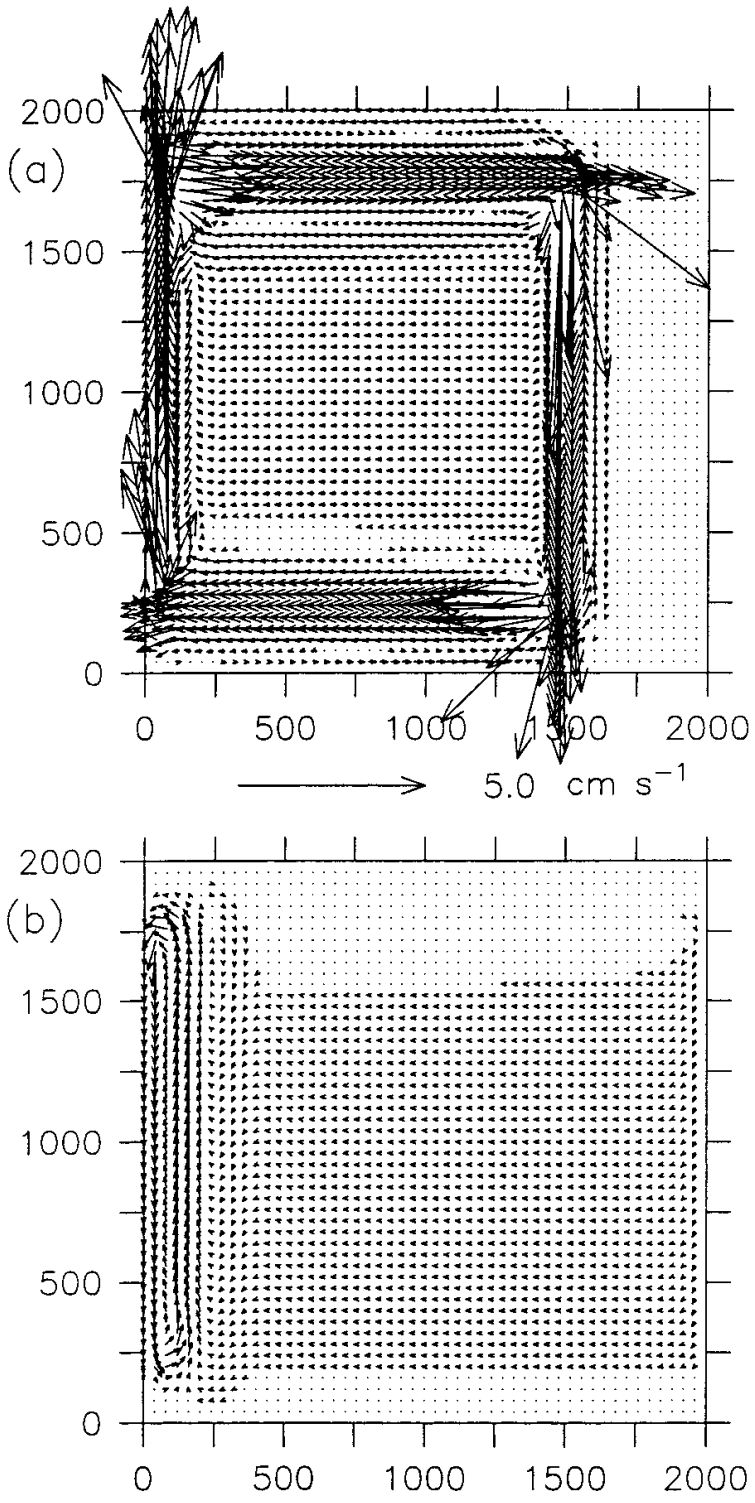

Figure 4. Large-scale circulation in the upper layer forced by a narrow band of upwelling from below located between 220 km $< y <$ 1780 km (only every other velocity point is shown). (a) Example of open ocean upwelling located at $x = 1500$ km. The strength of the large-scale recirculation $M_n/W = 3.82$, where W is the total amount of upwelled water. This is in close agreement with the theoretical estimate of $M_n/W = f_n/\beta L_y = 3.75$. (b) Upwelling confined to within 0.4δ of the eastern boundary. The recirculation is eliminated and flow is essentially zonal out of the upwelling region, in agreement with the analytic result (23).

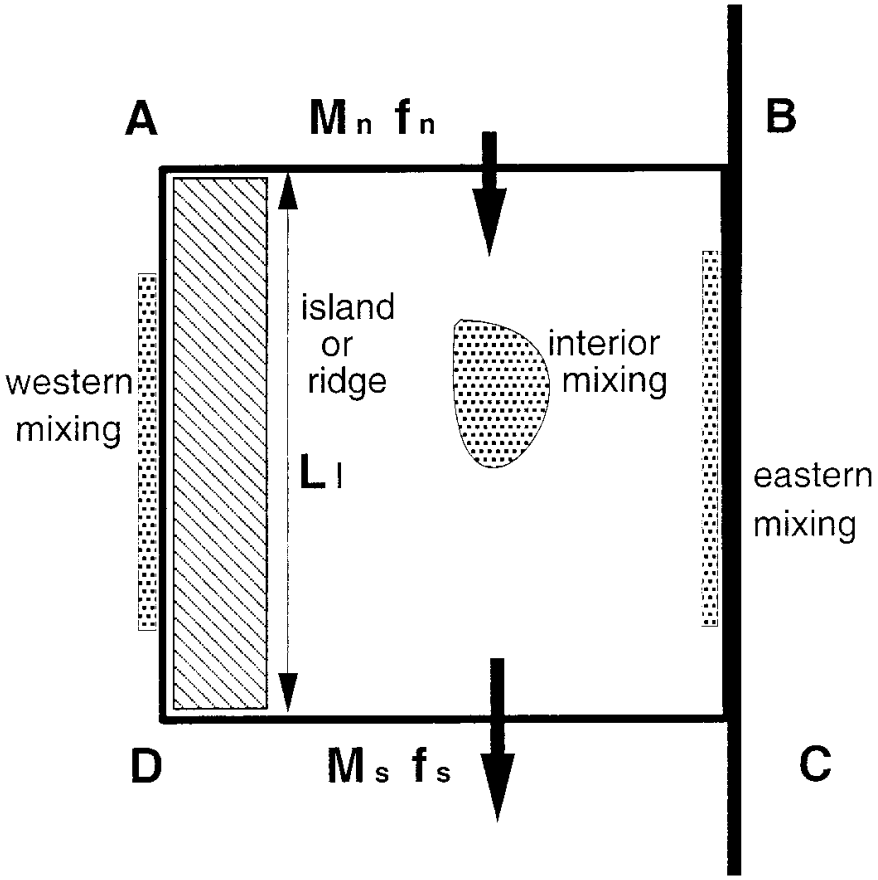

Figure 5. Schematic of the configuration with an island or mid-ocean ridge of meridional extent L_I. Three mixing scenarios are considered: mixing in the open ocean east of the island; mixing near the eastern boundary; and mixing along the western side of the island. Large-scale recirculations around the island are indicated by southward transport M_n at northern latitude of the island and southward transport M_s at the southern latitude of the island. Contour ABCDA is used to estimate the terms in the potential vorticity budget.

phy. The ideas developed in the previous section are now used to investigate the influences of diapycnal mixing on the mass flux between adjacent basins.

A schematic of the general problem of interest is shown in Figure 5. The basic influences of an island or topographic ridge are most clearly demonstrated by considering a simple rectangular island of meridional scale L_I. For simplicity, it is assumed that the zonal length scale of the island is less than or equal to the meridional length scale so that, in general, viscous effects on the northern and southern ends of the island are negligible, although the results here could easily be extended to allow for these effects (as in Pratt and Pedlosky, 1998). Three regions of diapycnal mixing will be considered: interior to the east of the island; adjacent to the eastern boundary of the basin; and adjacent to the western side of the island. As will be shown, the meridional length scale of the mixing region is not important for the mass transport around the island, although it is important for the circulation in the mixing basin.

a. Diapycnal mixing in the eastern basin

Following the approach in the previous section, let us consider the integral of the momentum equation tangent to the contour ABCDA in Figure 5. For interior mixing in the eastern basin, there is no source of potential vorticity within the contour and frictional effects along the contour are negligible. This is similar to the case of open ocean mixing except that the contour is now chosen to encompass the island, which is assumed to have meridional scale larger than the mixing region. This approach closely follows the traditional island rule of Godfrey (1989) and also used (although not explicitly stated) by Veronis (1973). It has the advantage that the dissipation along the eastern side of the island need not be known. Potential vorticity and mass budgets analogous to (7) and (9) require that upwelling east of the island results in a net circulation around the island of strength

$$M_n = \frac{f_s W}{\beta L_I}. \tag{26}$$

Note that the mass flux into and out of the eastern basin is contained entirely in the zonal jets M_n and M_s, the weak westward flow at intermediate latitudes for the open ocean upwelling is blocked by the island, and its pressure gradient is balanced by dissipation.

This is analogous to the traditional wind-driven island circulation discussed by Godfrey (1989), Wajsowicz (1993) and Pedlosky *et al.* (1997), among others, except that the wind-stress curl is replaced by the net upwelling in the eastern basin. The result is also very similar to (10) except that the meridional scale and the variation in the Coriolis parameter are now controlled by the scale of the island rather than the upwelling region. There will in general still be a recirculation in the eastern basin of strength given by (10); however, only a fraction ($L_y f_s / L_I f^*$), where f^* is the latitude of upwelling) of this will extend into the western basin. The dissipation along the eastern side of the island balances the planetary vorticity advection in the recirculation that is confined to the basin east of the island. The meridional and zonal scales of the mixing region, or its exact location, do not influence the transport between the eastern and western basins. The magnitude of the recirculation decreases as the equatorward end of the island approaches the equator ($f_s \to 0$). For the case where one end of the island is on the equator, any upwelling to the east of the island must flow out on the equatorward side of the island, and there will be no recirculation around the island forced by upwelling. Numerical calculations (not shown here) are in close agreement with (26).

b. Diapycnal mixing near the eastern boundary

If the mixing region is located near the eastern boundary of the basin, frictional effects become important along contour BC. In the limit of narrow upwelling ($L/\delta \leq O(1)$), the recirculation is eliminated and the mass flux is westward around both the northern and

southern ends of the island. The strengths of the transports are:

$$M_n = \frac{(f^* - f_s)W}{\beta L_I} \tag{27}$$

$$M_s = \frac{(f_n - f^*)W}{\beta L_I} \tag{28}$$

where f^* is a weighted average of the upwelling latitude

$$f^* = \frac{1}{W}\int_0^{L_I}\int_0^{L} fw\, dx\, dy. \tag{29}$$

For upwelling along the eastern boundary that is, on average, at the mid-latitude of the island, the westward flow around the island is uniformly split between the northern and southern passages.

c. Diapycnal mixing on the western side of the island

Perhaps the most interesting case is found when the upwelling (or downwelling) is located along the western edge of the island. This configuration is motivated in part by the recent estimates of strong diapycnal mixing along the western flank of the mid-Atlantic Ridge by Polzin *et al.* (1997). In addition, Godfrey and Ridgeway (1985) inferred that cooling and downwelling was taking place in the Leeuwin Current along the west coast of Australia. Integration of the momentum equation around the contour enclosing the island now introduces a viscous contribution along contour section DA of strength (23), (24), or (25) depending on the dissipation model. A recirculation around the island is required to balance this diffusive flux. Combining the mass budget (which requires $M_n = M_s = M$) with the circulation integral gives the strength of the circulation around the island. For no-slip boundary conditions, the recirculation strength is

$$M = \frac{f^* W}{\beta L_I}\frac{\delta}{L}\left[1 - \left(\cos\alpha - \frac{\sqrt{3}}{3}\sin\alpha\right)e^{-(L/2\delta)}\right]. \tag{30}$$

The recirculation strength with free-slip boundary conditions is

$$M = \frac{f^* W}{\beta L_I}\frac{\delta}{L}\frac{2\sqrt{3}}{3}e^{-(L/2\delta)}\sin\alpha. \tag{31}$$

The recirculation strength with linear bottom drag is

$$M = \frac{f^* W}{\beta L_I}\frac{\delta_s}{L}(1 - e^{-(L/\delta_s)}). \tag{32}$$

These are essentially the same as (23), (24), and (25) except that it is the meridional scale of the island that determines the recirculation strength rather than the meridional scale of

the mixing region. However, unlike the case of interior upwelling to the east of the island, the recirculation does depend on the latitude at which the mixing takes place. For very narrow mixing regions, the recirculation strength approaches $f^*W/\beta L_I$, independent of the meridional scale of the mixing or type of dissipation. The important result here is that diapycnal mixing on the western flank of a mid-ocean ridge or island can force a strong, large-scale recirculation between the western and eastern basins, even if the mixing is located far from the gaps that connect the deep basins.

One may also interpret the generation of a circulation around the island as a means to balance the momentum integral around the island itself. In the absence of local wind forcing, the integral of the viscous stress around the island must be zero. The upwelling along the western side of the island generates a stress of amplitude D, given by (23), (24), or (25). The only other location to develop significant stresses is on the eastern side of the island through a western boundary current. The stress in the western boundary current that balances the stress generated by the upwelling is just what is required to balance the meridional advection of planetary vorticity for a recirculation of strength (30), (31), or (32). It is somewhat surprising that dissipation on an eastern boundary with such weak flows (the western side of the island) balances the dissipation resulting from a generally much larger transport in the western boundary layer on the eastern side of the island.

d. Examples in a simple numerical model

A typical circulation forced by upwelling along the western side of the island is shown in Figure 6. An upwelling of strength 1 Sv is distributed uniformly along the western flank of the island with width 20 km with a Munk layer thickness of 50 km ($L/\delta = 0.4$). The meridional extent of the island is 1600 km, $f^* = 10^{-4}$ s^{-1}, $\beta = 2 \times 10^{-13}$ cm s^{-1}, giving $f^*/\beta L_y = 3.1$. The flow in the vicinity of the upwelling region is uniform and to the west, as found for the case with upwelling near the eastern boundary in the absence of an island. However, now the vorticity budget around the island requires a large scale recirculation, which clearly dominates the flow. The strength of the recirculation is 2.74 Sv, close to the theoretical estimate of 2.91 Sv from (30). The large-scale circulation around the island is independent of the meridional scale of the upwelling along the western edge of the island. Additional calculations (not shown here) indicate that, for localized sources, the latitude of the upwelling becomes important, as expected from (30).

The sensitivity of the recirculation strength to the meridional scale of the island is indicated by a series of numerical calculations in which the meridional scale of the island is varied between 400 km and 1600 km (Fig. 7a). There is generally good agreement with the theory, although the model recirculation is slightly weaker when $f^*/\beta L_I$ becomes large. This appears to be due to the westward- and eastward-flowing jets interacting to the west of the island as L_I becomes small.

The importance of the width of the upwelling region on the recirculation strength around the island is shown in Figure 7b. The island dimension is 1600 km, the Munk or Stommel layer thickness is 50 km. The strength of the recirculation around the island found in the

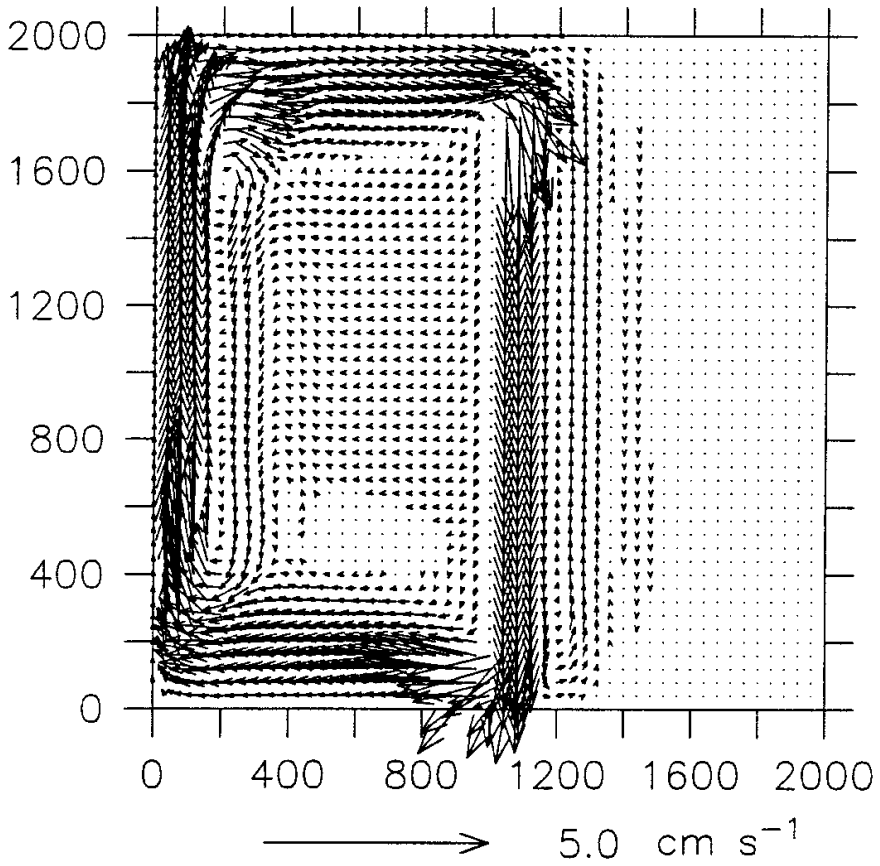

Figure 6. Large-scale circulation in the upper layer forced by upwelling from below of width 0.4δ along the western side of the island. The strength of the recirculation around the island compared to the upwelling strength $M/W = 2.74$, close to the theoretical estimate of 2.91 given by (30). Flow out of the upwelling region is very weak and toward the west. The position of the island is indicated by light shading at $x = 1000$ km.

model is shown for no-slip (squares) and free-slip (triangles) boundary conditions, as well as for linear bottom drag (circles), as a function of the upwelling width L/δ. There is generally close agreement between the model and theory, with the strongest recirculations around the island forced by the no-slip boundary conditions. However, the recirculation strength is independent of the specific form of dissipation as the upwelling width becomes small.

For large upwelling widths, the no-slip and bottom drag recirculation strength decays as δ/L, while the free-slip recirculation decays exponentially, as expected from the theory. In these cases, the dissipation contribution becomes negligible and the upwelling is balanced by the traditional β-plume recirculation confined to the western basin.

The abyssal basins are separated by narrow gaps, or fracture zones, in the mid-ocean ridge systems. The model has been configured to quantify how much transport can pass through the gaps as they become narrow. For simplicity, the zonal extent of the island is kept at 20 km. The gap width is controlled by short peninsulas extending from the basin perimeter toward the northern and southern tips of the island. The circulation is forced by a uniform upwelling along the western flank of the island. A typical circulation is shown in

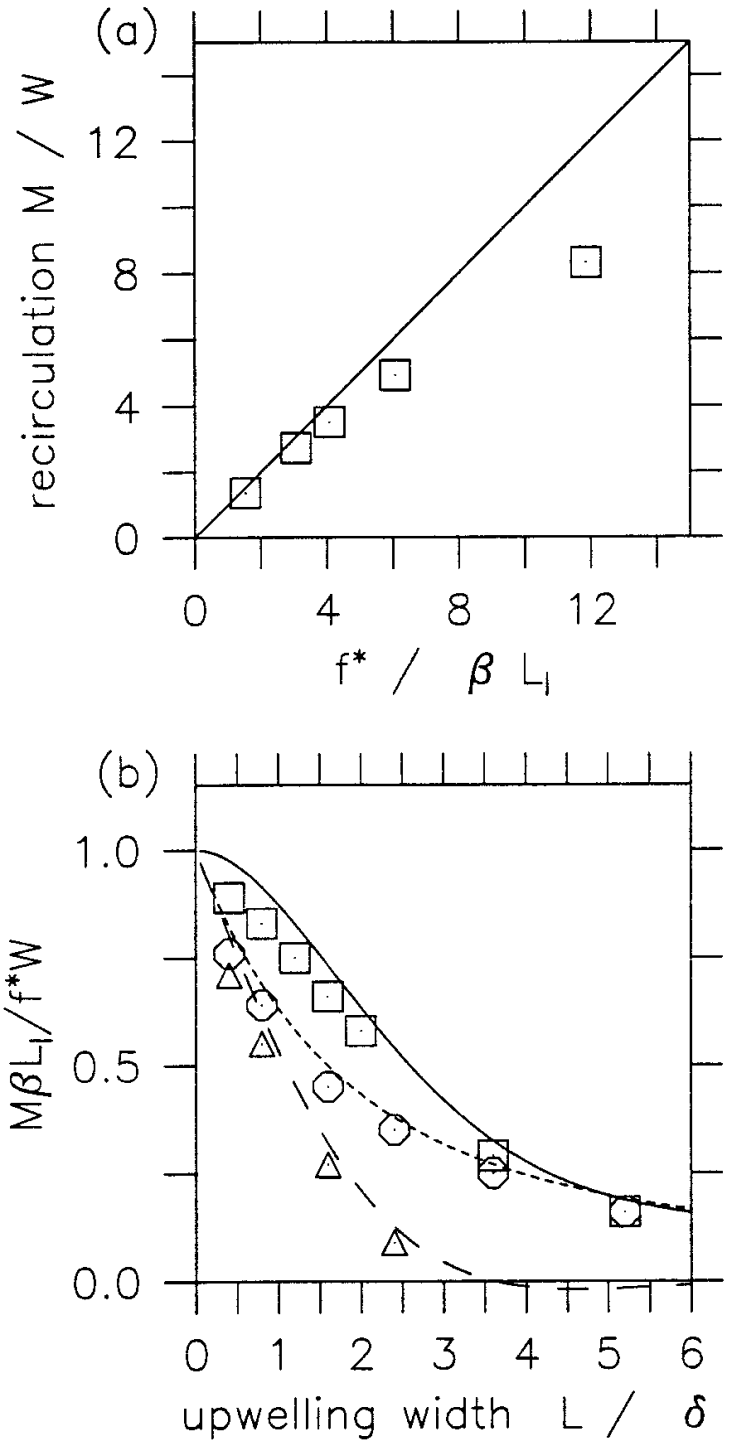

Figure 7. (a) Strength of the recirculation around the island found in the numerical model for various island lengths L_I ($f^*/\beta = 5 \times 10^6$ m, except the case with $f^*/\beta L_I = 1.5$, for which $f^*/\beta = 2.5 \times 10^6$ m). (b) Recirculation strength found in the model versus upwelling width L/δ for no-slip (squares), free-slip (triangles), and linear bottom drag (circles) dissipation. The simulated recirculation strength compares well with the theory given by (30) for no-slip (solid line), (31) for free-slip (long dashed line), and (32) for linear bottom drag (short dashed line).

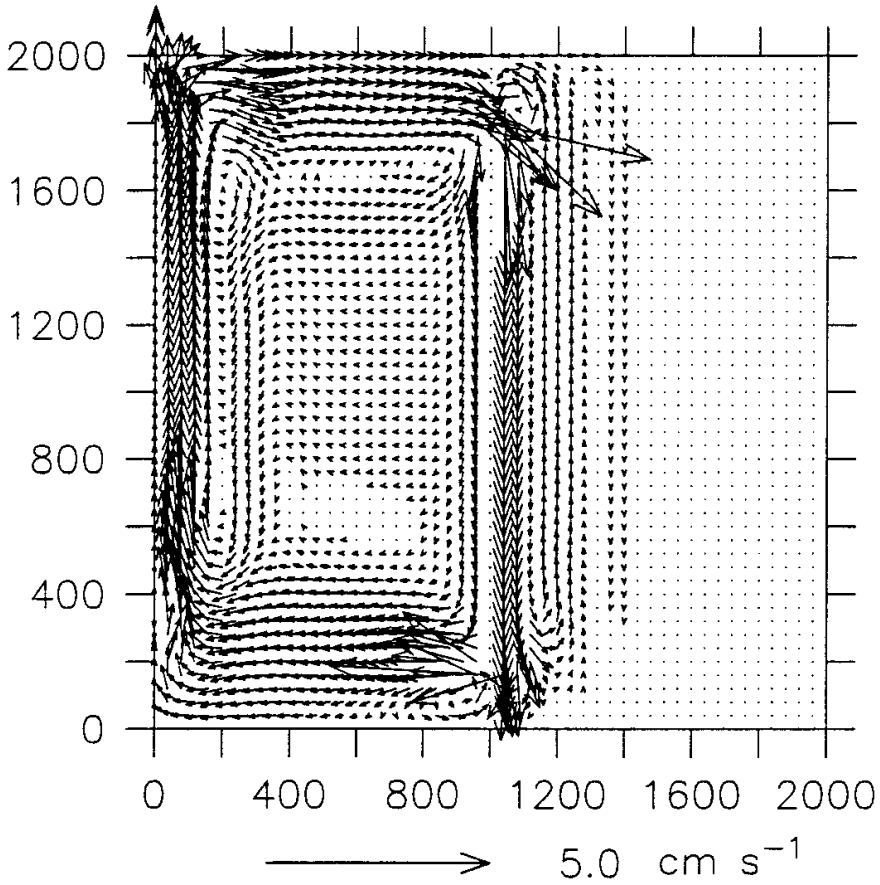

Figure 8. Large-scale circulation in the upper layer forced by upwelling from below, along the western side of the island with gap widths at the northern and southern tips of the island of $\Delta = 0.8\delta$. The total recirculation strength around the island in this case is approximately half the strength of the recirculation with very wide gaps. The position of the island and peninsulas are indicated by light shading at $x = 1000$ km.

Figure 8 for a gap width of $\Delta = 0.8\delta$. Even with this relatively narrow gap, there is still a considerable recirculation ($M/W = 0.51f^*/\beta L_I$) forced by the mixing on the western flank. The strength of the recirculation is shown as a function of gap width in Figure 9 for both no-slip (squares) and free-slip (triangles) boundary conditions. Flow is substantially impeded only when the gap width drops below δ. The transport is somewhat larger with free-slip boundary conditions as the gap width is decreased.

These transports are lower than would be expected from a simple estimate of the dissipation along the northern and southern boundary layers, which does not become important until $(\Delta/\delta)(L_I/L)^{1/3} \leq O(1)$, as discussed in PPSH. For the present configuration, $(L_I/L)^{1/3} = 4.3$ so that the transport through the gap is substantially reduced even when $(\Delta/\delta)(L_I/L)^{1/3} = O(5)$. The main difference compared to PPSH is that here the gap is defined by a peninsula whereas in PPSH it was defined by the distance between the island and the smooth basin perimeter. Circulation integrals around contour ABCDA show that the peninsula configuration experiences increased dissipation near the tips of the island compared to the case where the island extends toward the basin perimeter. This is likely due to the formation of additional meridional boundary layers along the peninsulas as the

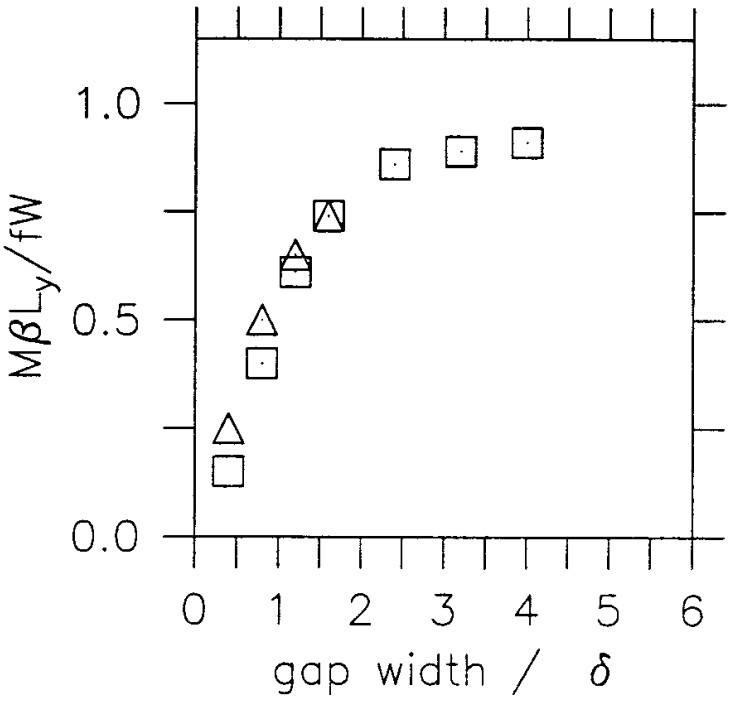

Figure 9. Normalized recirculation around the island as a function of gap width for no-slip (squares) and free-slip (triangles) boundary conditions.

flow approaches the narrow gaps, as suggested in Figure 8. This is only speculation, however, as quantifying the boundary layers near such corners is very difficult.

Strong mixing is known to occur in the narrow channels that pass from east to west in the mid-ocean ridge systems (i.e. Ferron *et al.,* 1998). Similar vorticity balances apply to this case, and a very similar recirculation gyre around the island is generated when the upwelling is confined to a point source within the gaps that connect the eastern and western basins.

For the case where one or both of the deep gaps inhibit free exchange between the basins, but the upper gaps do not, there will be a depth integrated circulation around the island. For such a case, the strength of the upper layer circulation will be as predicted for wide gaps, but the deep circulation will be reduced qualitatively similar to what is shown in Figure 9. The depth integrated circulation will then reflect the upper layer circulation, partially reduced in strength by the deep flow.

A similar situation occurs when the topography in one of the gaps is shallower than the depth in either basin but still allows some flow to pass through. If the ridge does not extend into the upper layer, then the circulation in the upper layer will be largely unaffected while the deep circulation will be partially blocked. The depth-integrated circulation will once again reflect the upper-layer circulation, partially reduced in strength by the deep flow. In this case, the advection of planetary vorticity around the island is balanced by the pressure drop across the partially blocked deep gap (see Wajsowicz, 1993). Although the pressure gradient is an exact differential and so must integrate to zero around any closed contour, the contribution to the circulation integral along contour direction s is $\int HP_s\, ds$. In the deep layer, the thickness H varies along the contour. The pressure change across the partial ridge

occurs at a thickness of approximately $H - h$, where h is the height of the ridge, while the compensating pressure change along the remainder of the contour interval occurs at thickness near H, so that the integral around the closed contour does not vanish.

Topography can also influence the depth integrated flow if the bottom slopes approaching the island. There are two consequences of having a weak sloping bottom. Weak in this context indicates that the isopycnals do not intersect the bottom and the topographic β is less than or equal to the planetary β. The first is that there will generally be a stretching or compression of the deep layer if the flow crosses the topography. Unlike the upwelling provided at the isopycnal interface, this stretching acts as a potential vorticity source because there is no vertical mass flux to compensate for the stretching in the potential vorticity budget. For the case of upwelling imposed along the western flank of an island and a topography that shoals as one approaches the island from the west, the zonal flow into the upwelling region in the deep layer will provide compression over the zonal scale of the topography, L_T. For the case of narrow mixing ($L \ll L_T$), the amplitude of the topographically induced upwelling is

$$W_T = \frac{h}{H} W, \tag{33}$$

for $h \ll H$, where h is the height of the topography and H is the thickness of the lower layer. The barotropic flow that will result satisfies the usual barotropic vorticity equation near an eastern boundary subject to forcing (33) over the zonal extent L_T and the meridional extent of the forcing W. For upwelling near the topography, $W_T > 0$ and the barotropic flow will be southward over the sloping bottom. The influence of dissipation will still be governed by (30), (31), or (32) where L is replaced by L_T. This barotropic flow will generally be smaller than the baroclinic flow around the island, scaling as

$$\frac{M_T}{M} = \frac{h}{H}. \tag{34}$$

The second major influence of a sloping bottom is to shift the deep potential vorticity contours that extend away from the mixing region relative to those in the upper layer. In the linear limit, the upper layer potential vorticity contours are dominated by the planetary vorticity gradient β and are thus zonal. The sloping bottom will increase the potential vorticity of the deep layer as one approaches the island from the west so that the contours will be diverted toward the south. In the limit of weak friction, the flow outside the forced upwelling region will be along potential vorticity contours in both layers. The flow in the upper layer will remain zonal (as shown, for example, in Fig. 6), while the deep flow will follow the potential vorticity contours that are deflected meridionally over the sloping bottom. For weak bottom topography, the net result is to meridionally shift the deep zonal jets that feed the circulation around the island. The resulting depth integrated flow is then dominated by two narrow recirculation gyres extending toward the west from the northern

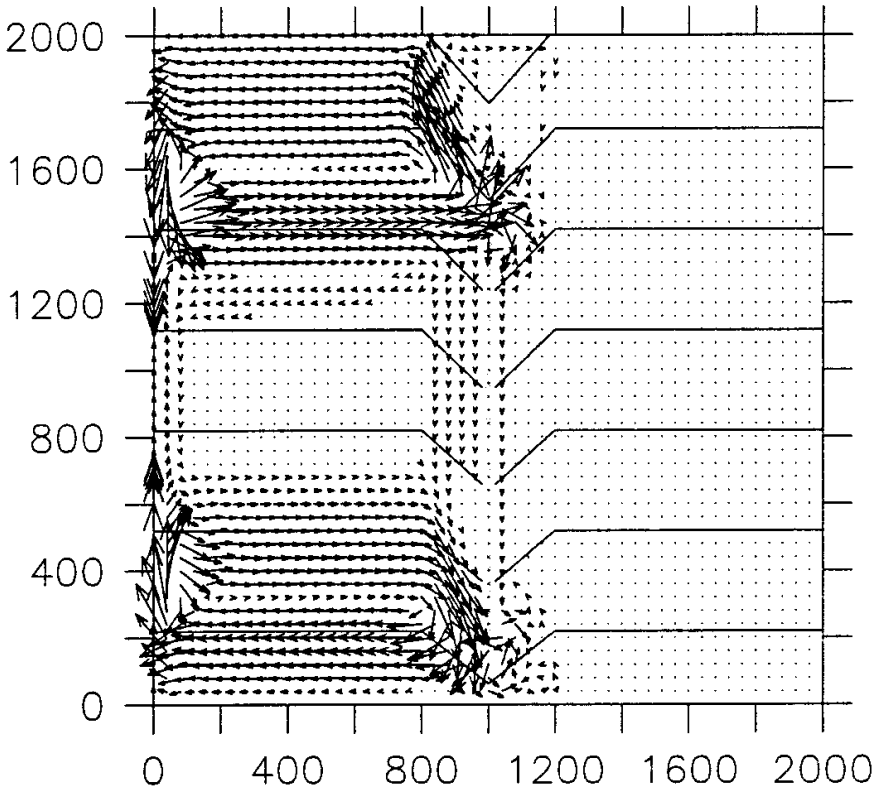

Figure 10. The depth integrated transport for a case with narrow upwelling along the western side of the island and a uniform bottom slope of 3.75×10^{-4} extending 200 km eastward and westward from the ridge. The deep flow is diverted relative to the upper layer flow because of the alteration of potential vorticity contours in the deep layer (the barotropic potential vorticity contours are given by the solid lines).

and southern tips of the island. An example of this is shown in Figure 10 for a case with uniform upwelling along the western side of the island and a topographic slope of 3.75×10^{-4} and width 200 km (maximum height 75 m). The strength of the depth integrated recirculation gyres is the same as the baroclinic recirculation around the island provided the topographic height exceeds

$$h > \frac{\delta\beta}{f} H. \tag{35}$$

For more realistic bottom slopes of $O(10^{-3})$, the deep potential vorticity contours are nearly coincident with depth contours around the deep basin perimeter. Spall (2000) has recently considered the large-scale circulation forced by diapycnal mixing over a steeply sloping topography. It is shown that sufficiently strong bottom slopes result in stretching at the bottom that just balances the diapycnal mass flux. In these cases, the strong deep recirculation found with a flat bottom is replaced by a weak flow along the topography into or out of the mixing region, while the strong horizontal recirculation in the upper ocean remains.

4. Summary

The dynamics of narrow upwelling and downwelling regions in simply and multiply connected domains are investigated using both analytic and numerical methods. The primary motivations for this study are the recent observational and theoretical results that suggest that dominant components of both the upwelling and downwelling limbs of the thermohaline circulation take place in narrow regions adjacent to topography. It is shown that frictional effects become important to leading order in the large-scale potential vorticity budget as the vertical motions are confined to regions adjacent to boundaries that are on the order of the relevant boundary layer thickness or less (both lateral viscosity and linear bottom drag solutions are provided here). The large-scale circulation that is required to balance the flux of planetary vorticity out of the upwelling region is strongly dependent on its proximity to a lateral boundary. In the open ocean, horizontal recirculation gyres are generated that are typically much stronger than the upwelling strength. As the upwelling is confined near a boundary, however, viscous dissipation replaces the contribution of the horizontal recirculation in the potential vorticity budget. For narrow regions of vertical motion, the recirculation is eliminated and the large-scale flow is unidirectional along potential vorticity contours out of (into) the upwelling (downwelling) region.

For cases where the upwelling is adjacent to the western side, or anywhere to the east, of an island or mid-ocean ridge, a large-scale recirculation around the island is required. This general response is independent of the details of the mixing region. Simple momentum and mass budgets around the island are used, together with a boundary layer solution for narrow upwelling adjacent to a boundary, to estimate the strength of the recirculation based on the latitude and meridional scale of the island. For typical mid-latitude, planetary-scale topographic features, the recirculation around the island can be several times larger than the strength of the upwelling. The addition of a weak sloping bottom adjacent to the boundary modifies the deep potential vorticity contours and results in a net depth-integrated circulation, although the basic dynamics in each of the layers remain similar to the flat bottom case.

These results provide a dynamical link between the narrow regions through which most of the meridional overturning circulation passes vertically and the large-scale, nearly horizonal circulation that connects these upwelling and downwelling regions. The very simple approach adopted here, although quite idealized with respect to the real ocean, allows one to infer many general consequences of vertical motions and illuminates the fundamental role that the meridional gradient of planetary vorticity and lateral boundaries plays in closing the three-dimensional circulation.

Acknowledgments. Support for this work was provided by the National Science Foundation under Grant OCE-9818337 and by the Office of Naval Research under Grant N00014-97-1-0088. This work has benefitted from numerous interesting and helpful conversations with Joseph Pedlosky. Comments and suggestions from George Veronis helped to improve the presentation. This is Woods Hole Oceanographic Institution contribution number 10152.

REFERENCES

Armi, L. 1978. Some evidence for boundary mixing in the deep ocean. J. Geophys. Res., *83,* 1971–1979.

Bleck, R., C. Rooth, D. Hu and L. T. Smith. 1992. Salinity-driven thermocline transients in a wind- and thermohaline-forced isopycnal coordinate model of the North Atlantic. J. Phys. Oceanogr., *22,* 1486–1505.

Ferron, B., H. Mercier, K. Speer, A. Gargett and K. Polzin. 1998. Mixing in the Romanche Fracture Zone. J. Phys. Oceanogr., *28,* 1929–1945.

Godfrey, J. S. 1989. A Sverdrup model of the depth-integrated flow for the World Ocean allowing for island circulations. Geophys. Astrophys. Fluid Dyn., *45,* 89–112.

Godfrey, J. S. and K. R. Ridgeway. 1985. The large-scale environment of the poleward-flowing Leeuwin Current, Western Australia: Longshore steric height gradients, wind stresses and geostrophic flow. J. Phys. Oceanogr., *15,* 481–495.

Jia, Y. 2000. The formation of an Azores Current due to Mediterranean overflow in a modelling study of the North Atlantic. J. Phys. Oceanogr., *30,* 2342–2358.

Joyce, T. M. and K. G. Speer. 1987. Modeling the large-scale influence of geothermal sources on abyssal flow. J. Geophys. Res., *92,* 2843–2850.

Ledwell, J. R. and B. M. Hickey. 1995. Evidence for enhanced boundary mixing in the Santa Monica Basin. J. Geophys. Res., *100,* 20,665–20,679.

Ledwell, J. R., A. J. Watson and C. S. Law. 1993. Evidence for slow mixing across the pycnocline from an open ocean tracer-release experiment. Nature, *364,* 701–703.

Marotzke, J. 1997. Boundary mixing and the dynamics of three-dimensional thermohaline circulations. J. Phys. Oceanogr., *27,* 1713–1728.

Munk, W. H. 1966. Abyssal recipes. Deep-Sea Res., *13,* 707–730.

Özgökmen, T. M., E. P. Chassignet and C. G. H. Rooth. 2000. On the connection between the Mediterranean outflow and the Azores Current. J. Phys. Oceanogr. (submitted).

Pedlosky, J. 1987. Geophysical Fluid Dynamics, Springer-Verlag, 710 pp.

—— 1996. Ocean Circulation Theory. Springer, Berlin, 453 pp.

Pedlosky, J., L. J. Pratt, M. A. Spall and K. R. Helfrich. 1997. Circulation around islands and ridges. J. Mar. Res., *55,* 1199–1251.

Polzin, K. L., J. M. Toole, J. R. Ledwell and R. W. Schmitt. 1997. Spatial variability of turbulent mixing in the abyssal ocean. Science, *276,* 93–96.

Pratt, L. J. and J. Pedlosky. 1998. Barotropic circulation around islands with friction. J. Phys. Oceanogr., *28,* 2148–2162.

Price, J. F. and M. O'Neil Baringer. 1994. Outflows and deep water production by marginal seas. Prog. Oceanogr., *33,* 161–200.

Schmitz, W. J. and M. S. McCartney. 1993. On the North Atlantic circulation. Rev. Geophys., *31,* 29–49.

Spall, M. A. 1999. A simple model of the large-scale circulation of Mediterranean Water and Labrador Sea Water. Deep-Sea Res. II, *46,* 181–204.

—— 2000. Large-scale circulations forced by mixing over a sloping bottom. J. Phys. Oceanogr. (submitted).

Spall, M. A. and R. S. Pickart. 2000. Where does dense water sink? A subpolar gyre example. J. Phys. Oceanogr. (in press).

Stommel, H. M. 1982. Is the South Pacific helium-3 plume dynamically active? Earth Planet. Sci. Lett., *61,* 63–67.

Toole, J. M., R. W. Schmitt, K. L. Polzin and E. Kunze. 1997. Near-boundary mixing above the flanks of a midlatitude seamount. J. Geophys. Res., *102,* 947–959.

Veronis, G. 1973. Model of the world ocean circulation, 1, Wind-driven two-layer. J. Mar. Res., *31,* 228–288.

Wajsowicz, R. C. 1993. The circulation of the depth-integrated flow around an island with application to the Indonesian throughflow. J. Phys. Oceanogr., *23,* 1470–1484.

Yang, J. and J. F. Price. 2000. Water-mass formation and potential vorticity balance in an abyssal ocean circulation. J. Mar. Res., *58,* 789–808.

Received: *6 April, 2000;* revised: *20 August, 2000.*